Title: Worldwide moderate-resolution mapping of lake surface chl-a reveals variable responses to global change (1997-2020)

Authors: Benjamin M. Kraemer[1]*, Karan Kakouei[1], Catalina Munteanu[2], Michael W. Thayne[1,3,4], Rita Adrian[1,3]

*Corresponding author: ben.m.kraemer@gmail.com

[1] IGB Leibniz Institute for Freshwater Ecology and Inland Fisheries, Berlin, Germany
[2] Albert-Ludwigs-University of Freiburg, Freiburg, Germany
[3] Freie Universität of Berlin, Berlin, Germany
[4] University of Geneva, Geneva, Switzerland

Abstract:

Anthropogenic activity is leading to widespread changes in lake water quality--a key contributor to socio-ecological health. But, the anthropogenic forces affecting lake water quality (climate change, land use change, and invasive species) are unevenly distributed across lakes, across the seasonal cycle, and across space within lakes, potentially leading to highly variable water quality responses that are poorly documented at the global scale. Here, we used 742 million chlorophyll-a (chl-a) observations merged over 6 satellite sensors (daily, 1 to 4 km resolution) to quantify water quality changes from 1997 to 2020 in 345 globally-distributed large lakes. Chl-a decreased across 56% of the cumulative total lake area, challenging the putative widespread increase in chl-a that is expected due to human activity. 18% of lakes exhibited both significant positive and significant negative chl-a trends across different locations or times of the year. This spatiotemporal complexity demonstrates the value of moderate resolution mapping of lake chl-a to inform water management decision-making and to determine the local ecological consequences of human activity.

Main text:

Nutrient pollution and climate change may increase lake chl-a concentrations through various direct and indirect pathways [1,2]. For instance, industry, agriculture, and urbanization has caused well-documented increases in chl-a by delivering nutrients to lakes through runoff and atmospheric deposition[1]. In addition, climate change can increase chl-a through the temperature dependence of primary production [3], by expanding the stratified season [4], or by promoting lake conditions which favor bloom-forming algae [5–7]. Land use and climate change can interact leading to synergistic increases in chl-a concentrations[8] with potential negative consequences for the millions of people who depend on lakes for their livelihoods [9].

However, global change is also associated with decreases in lake chl-a in some contexts. Climate change has been shown to reduce chl-a by impeding the entrainment of deep water nutrients into the surface waters where it is available to support algae growth [10–12] particularly in nutrient-poor lakes[13,14]. Increased temperatures may also reduce chl-a when temperature-induced increases in the consumption and degradation of algae outpace temperature-induced increases in algal production [15,16]. Invasive species can affect chl-a indirectly through trophic cascades or directly by grazing. For instance, invasive filter feeding mussels reduce chl-a by rapidly filtering lake water [17,18]. Localized reductions in aquatic nutrient pollution can also reduce chl-a [19–21].

These environmental changes are unevenly distributed across lakes, across the seasonal cycle, and across space within lakes, potentially leading to highly heterogeneous water quality responses [1]. But this heterogeneity is not yet well-captured at the global scale. Thus, it remains uncertain whether the environmental changes operating a global scale tend to increase or decrease chl-a. An understanding of global patterns and spatial heterogeneity in long-term changes in lake water quality at sufficient spatiotemporal resolution is necessary for improving our macroecological understanding of lake ecosystems in a rapidly changing world. This improved understanding would also allow managers to design and implement more precisely targeted restoration strategies that are ultimately more effective at safeguarding lake resources [22].

Past global syntheses of long-term trends in chl-a at the global scale have treated lakes as discrete units with homogenous spatiotemporal changes [2,14]. Here, we use a less discretized approach [23] focusing on within-lake changes at the daily temporal scale and at moderate spatial resolution (1km spatial resolution for Europe and 4 km spatial resolution for the rest of the world). We used 742 million chl-a observations merged across 6 satellite sensors (SeaWiFS, MODIS AQUA, MERIS, OLCI-B, VIIRS NPP, and VIIRS JPSS-1) to assess long-term trends in 345 large lakes (surface area greater than 100 km^2) under ice-free and cloud-free conditions from 1997 to 2020. To detect chl-a, we used algorithms developed for coastal and inland waters[24] which we adapted for specific lakes according to their mean depth, surface area, and shoreline complexity using Boosted Regression Trees (BRTs). This lake-specific algorithm tuning approach was based on cross validation comparing remote sensing and *in situ* chl-a data in 56 lakes where a total of 20,165 *in situ* chl-a observations were available. We estimated the uncertainty in chl-a trends using bootstrapped error propagation techniques [25] incorporating the uncertainty in the chl-a algorithm and the lake-specific algorithm tuning approach.

We found that when chl-a trends were calculated as lake-wide averages, the median chl-a trend across all lakes was +0.04 μg chl-a $decade^{-1}$ (total range = -11.98 to +9.64 μg chl-a $decade^{-1}$, interquartile range = -0.03 to 0.27 μg chl-a $decade^{-1}$; Fig. 1). Lake-wide average chl-a increased in 63% of lakes (225 out of 345; Fig. 2) and decreased in the remaining 37%. Trends were statistically significant in 63% of the increasing trends and 57% of the decreasing trends at the 0.1 level ($\alpha = 0.1$). Thus, more lakes had significant trends than what would be expected based on chance alone and this was true regardless of which arbitrary threshold was used for statistical significance testing (we tested $\alpha = 0.1, 0.05, 0.01$). These general findings are comparable to previous work based on Landsat imagery which found that 68% of large lakes had increasing chl-a concentrations and 39% of lakes had statistically significant trends (alpha = 0.1) in chl-a since the 1980's [2].

The lake-wide average trends agreed well with published literature on phytoplankton, chl-a, and other phytoplankton proxies based on *in situ* data sources. For example, *in situ* chl-a has decreased in Lake Nicaragua (Cocibolca) after nutrient pollution peaked there in the mid 2000s [26] (Fig. 1). *In situ* phytoplankton biomass proxies also decreased in Lake Tanganyika as enhanced thermal stratification due to climate change has reduced primary production [10,11,27] (Fig. 1). Conversely, chl-a variation in Lake Kivu shown here (Fig. 1) matched a strong cycle in phytoplankton biomass observed *in situ* due to background climate variation [28] . Remotely-sensed chl-a also increased in Lake Erie which has experienced a well-documented nutrient pollution trend for decades due to agricultural expansion and intensification[29] (Fig. 1).

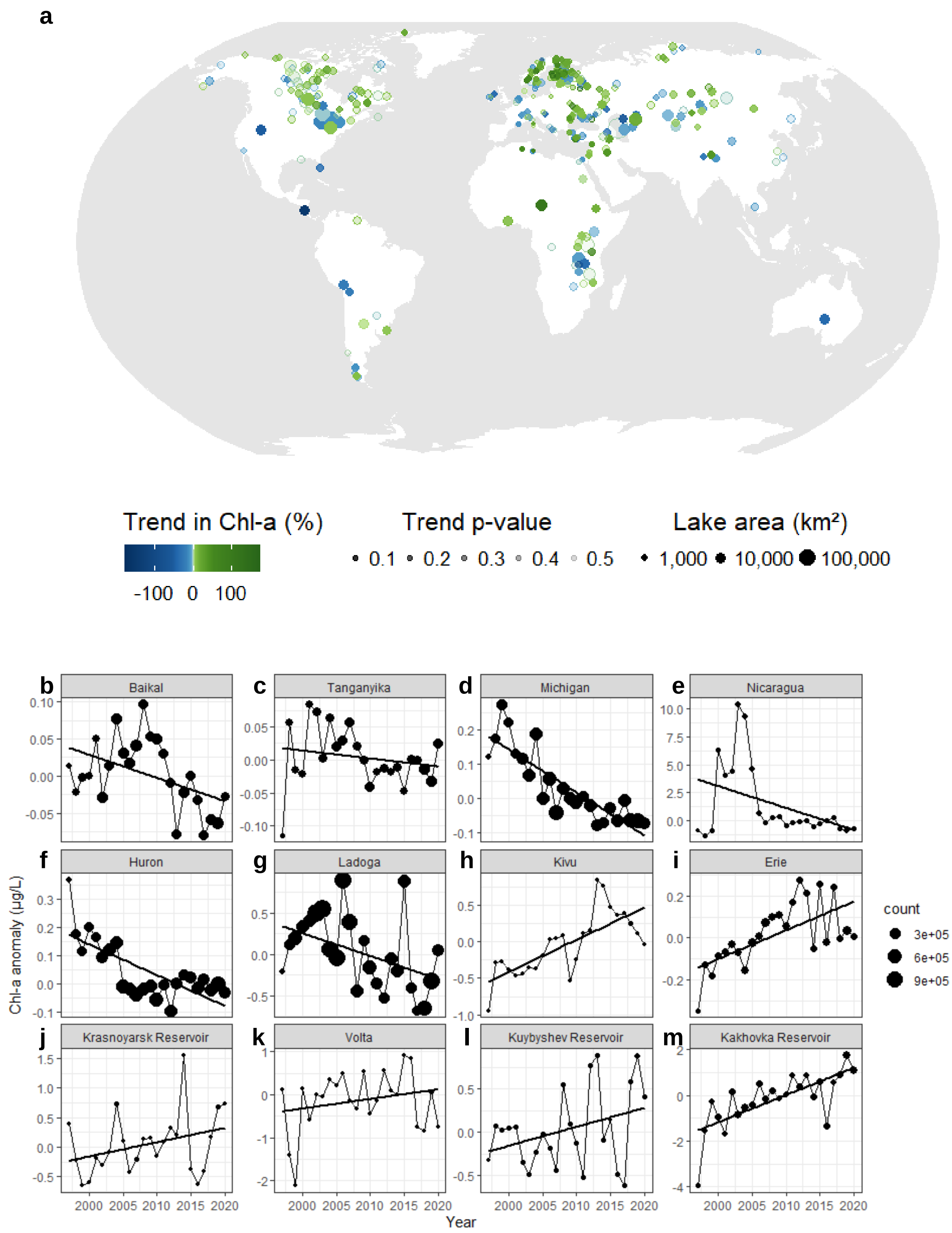

Fig. 1 | Chl-a percent change (1997-2020) based on lake-wide averages. Map showing lake-wide trends for 345 globally distributed lakes where the sizes of the dots are proportional to the size of the lake and the transparency of the dot is proportional to the significance of the trend (**a**). Time series show the chl-a anomalies for the 6 lakes with the largest negative trends (**b:g**) in lake-wide chl-a and the 6 lakes with the largest positive trends (**h:m**) in lake-wide chl-a when trends were weighted by each lake's volume. The black lines (**b:m**) are the ordinary least squares regression line and the size of the dots represents the number of remote sensing observations in each year (**b:m**). An inset map of Europe can be found in Supplemental Fig. S1.

While 63% of lakes had positive chl-a trends at the lake-wide average scale, only 44% of the total lake area experienced increases in chl-a at the pixel scale. This difference arose because chl-a tended to decrease in the largest lakes (Fig 1). The global median chl-a trend was -0.01 μg chl-a decade^{-1} when pixel-level trends were weighted by pixel area (pixel area varies across latitude when a consistent equal angle grid is applied). In total, we investigated chl-a trends at the pixel scale for 1,383,893 km^2 of cumulative lake area. Chl-a increased for 612,014 km^2 of the cumulative lake area and 17% (104,871 km^2) was significant at the 0.1 level. Chl-a decreased across 771,879 km^2 of the cumulative lake area and 19% (148,175 km^2) of the lake area with decreasing trends was significant at the 0.1 level. Thus, more lake area had significant trends at the pixel scale than what would be expected based on chance alone regardless of which arbitrary threshold was used for statistical significance (we tested α = 0.1, 0.05, and 0.01). This finding challenges the broadly held assumption that global change causes widespread increases in lake chl-a [1].

Decreases in chl-a observed here have been attributed to water management efforts in some lakes (e.g. Ladoga [30]), and to invasive filter feeding mussels in others (e.g. Ontario, Huron, Michigan [20]), but these drivers alone cannot explain decreases across all lakes. Decreases in chl-a as a result of climate change through changes to terrestrial inputs [31], higher heterotrophic consumption of algae [32,33], or climate change mediated reductions in deep water nutrient entrainment to the well-lit surface waters [4,34–36] may be an underrecognized response to global change. While this result is most relevant for Earth's large lakes, widespread bluing trends have been observed in small lakes as well [31,37,38]. We recommend future emphasis on how global-change may reduce chl-a, especially because chl-a reductions can heavily affect lake ecosystems and the benefits that humans derive from them [19–21].

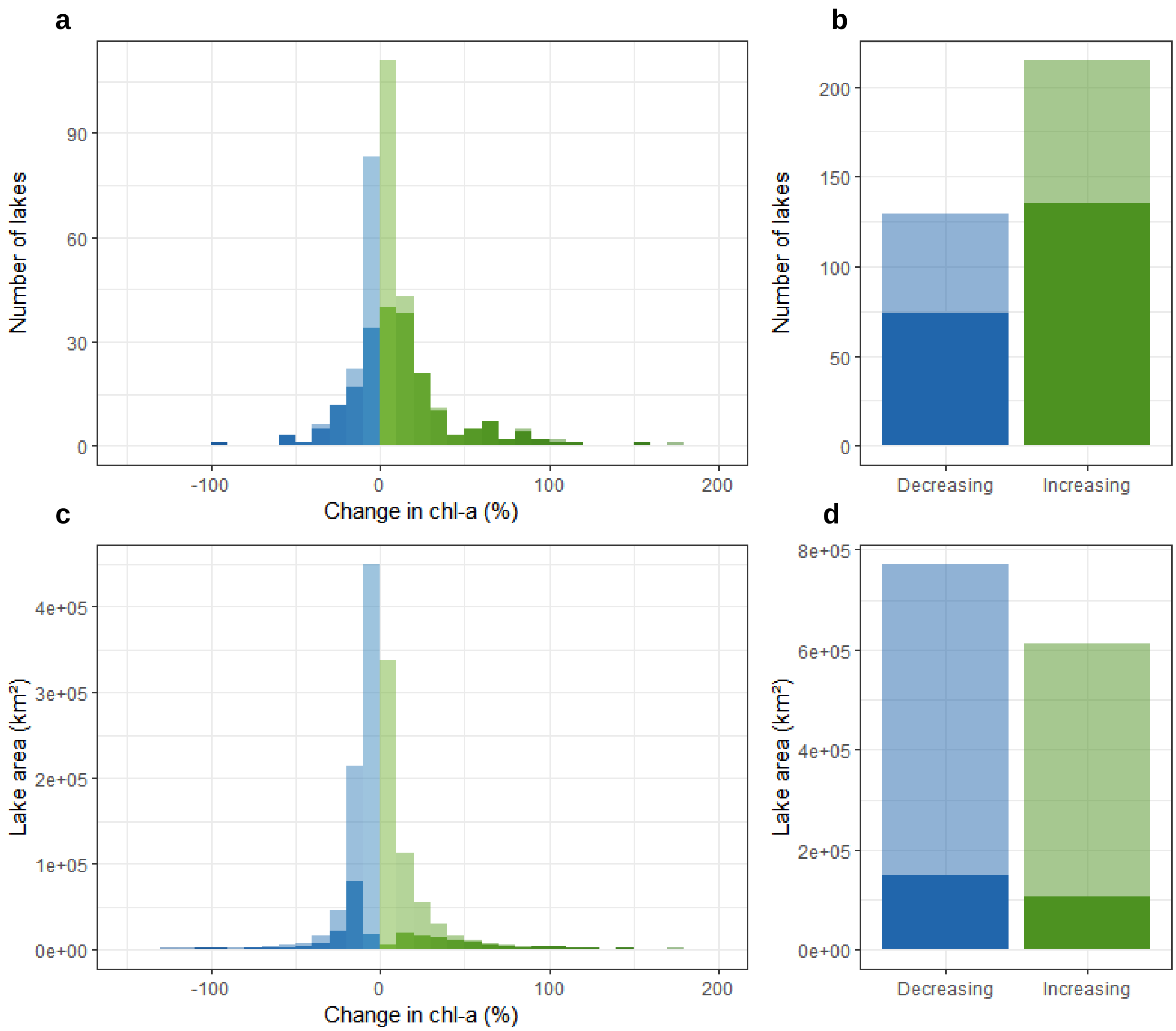

Fig. 2 | Distribution of global chl-a percent change (1997-2020). Percent change at the lake-wide average scale (**a**, **b**), and at the lake area scale (**c**, **d**). Blue indicates decreasing trends and green indicates increasing trends. The solid colors represent trends significant at the $\alpha = 0.1$ level.

Long-term trends based on lake-wide averages hid the complexity of long-term change in chl-a across lake surfaces. Some lakes which had weak or no significant overall chl-a trend at the lake-wide scale, had strong simultaneous increases and decreases in chl-a at different locations within the lake (Fig. 3). For example, the Caspian Sea had a weak overall trend at the lake-wide scale but chl-a increased significantly in the northern shallows (Fig. 3). Increasing trends in the Caspian Sea primarily occurred near the inflowing Ural, Volga, and Terek rivers which deliver large nutrient loads from the surrounding landscape [39] (Supplemental Fig. S2). At the lake-wide scale, this increase in chl-a in the northern shallows was offset by the statistically weaker but widespread decrease in chl-a in the deeper offshore areas (Fig. 3).

In addition to the Caspian Sea, many other lakes experienced local increases in chl-a in the shallower areas closer to the shore near inflowing rivers that diverged from lake-wide average trends (Fig. 3). For example, Lake Huron experienced very localized increases in chl-a in the shallow Saginaw Bay where the Saginaw River enters the lake bringing with it a variety of agricultural and industrial pollutants [40] (Supplemental Fig. S2). At the same time, chl-a decreased in the offshore deeper areas of Lake Huron where the combined effect of nutrient mitigation and invasive species expansion has caused reductions in chl-a [20]. Lake Titicaca experienced very localized increases in chl-a in the smaller south east basin where inflowing rivers drain an increasingly urbanized catchment near El Alto/La Paz, Bolivia [41] (Supplemental Fig. S2). A strong reduction in chl-a concentrations in Lake Ladoga (Fig. 3) suggests that continued efforts at reducing nutrient pollution have improved water quality there. However, patchy greening areas in the shallower parts of Lake Ladoga may indicate the potential for internal re-suspension of past phosphorus loads resting in the sediment [42]. Lake Nasser/Nubia, one of the largest manmade lakes in the world, has a pronounced greening trend near the inflowing Nile River which transitions into a bluing trend near the outflow of the reservoir. This pattern of chl-a increases transitioning to chl-a decreases was common in large reservoirs presumably because nutrient loads from incoming rivers get diluted as they pass into larger volumes of water with greater thermal stratification. Thus, simultaneous increases and decreases in chl-a for specific locations within lakes can reflect differences in the location and strength of various anthropogenic stressors affecting chl-a. Chl-a changes at the local scale within lakes may diverge widely from the lake-wide average.

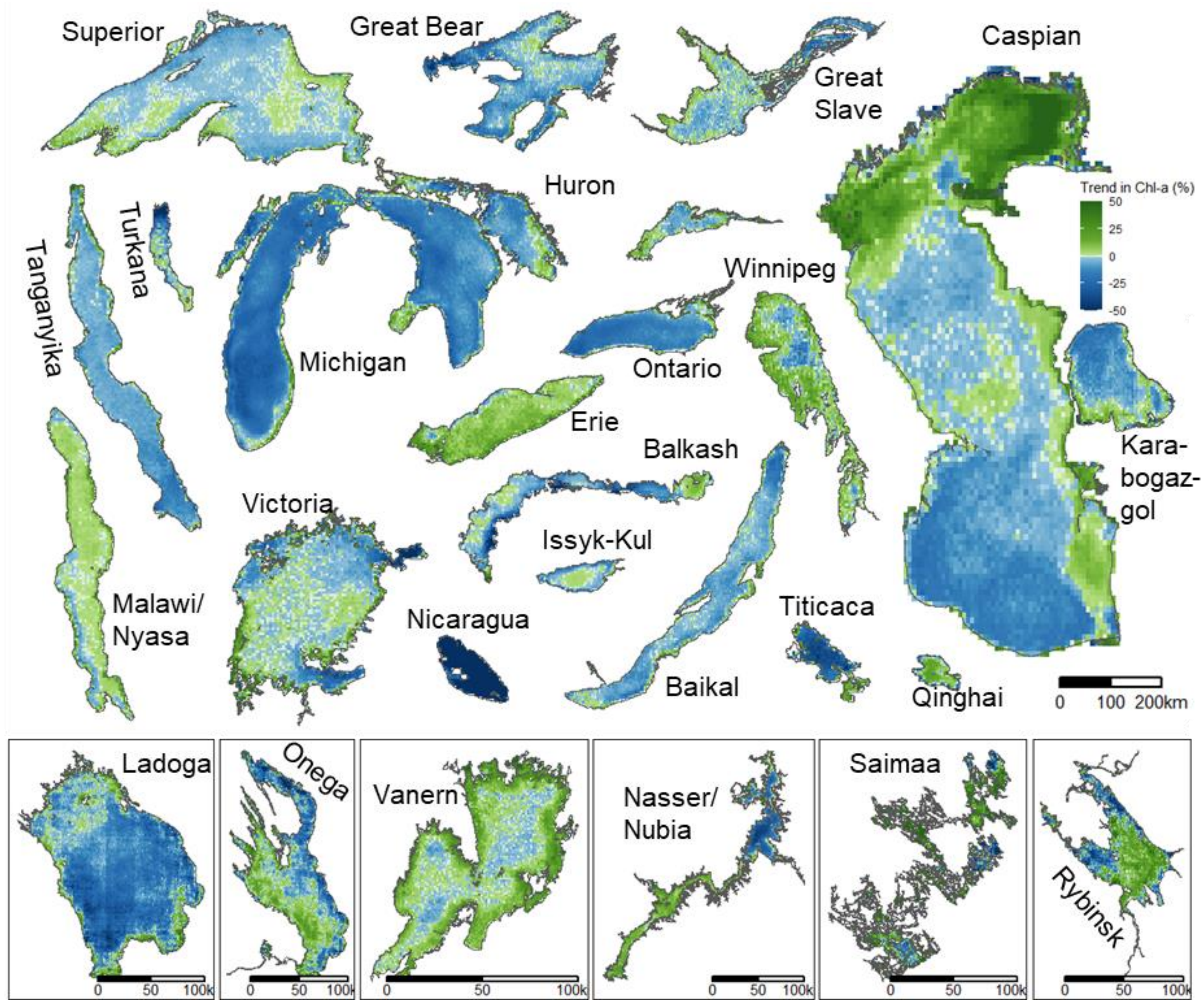

Fig. 3 | Spatial variation within and across lakes in chl-a trends (1997-2020). The relative positions of the lakes shown here do not reflect geo-spatial location but lake sizes share a common scale except where indicated otherwise in the boxed insets. Lakes shown are those with the largest number of chl-a observations. The p-values associated with each grid cell can be found in Supplemental Fig. S3.

Long-term trends based on lake-wide averages also failed to capture the complexity of long-term change in lake surface chl-a across days of the year for individual lakes. For example, in Lakes Michigan, Huron, and Ontario, introduced mussels have reduced chl-a primarily in the less stratified times of the year when the impact of filter feeding on phytoplankton is strongest [18] (Fig. 4). Chl-a decreases in Lake Tanganyika were most pronounced during the dry season when climate change mediated changes to stratification patterns have dampened seasonal mixing [10,11]. Several lakes had serial increases and decreases in chl-a across the seasonal spectrum (Fig. 4). For instance, earlier seasonal stratification in Lake Superior due to climate change may have increased chl-a in early spring when phytoplankton benefit from being retained in the well-lit stratified surface layer where they can better photosynthesize. But the increased chl-a in early spring is combined with a summer decrease in chl-a as prolonged summer stratification reduces the amount of nutrients available for primary producers[43].

This within lake complexity (Fig. 3, Supplemental Fig. S4) and seasonal complexity (Fig. 4) of chl-a trends discounts the tendency to emphasize the dichotomous view that lakes are either undergoing increases or decreases in chl-a. 18% of lakes exhibited significant positive and negative trends in chl-a at different locations or at different times of the year (more than 10% of positive trends and more than 10% of the negative trends had p-values less than 0.1). This combination of positive and negative trends for individual lakes highlights the heterogeneity of lake responses to global change. Therefore, lake ecology and ecosystem management should recognize the potential for local changes at specific times of the year to vary widely from lake-wide averages. Whole-lake chl-a trends can mask spatiotemporal trend variability leading to lakes with weak trends at the lake-wide scale but strongly contrasting increases and decreases in chl-a at finer seasonal and spatial resolution (e.g. Caspian Sea in Fig. 3 and Fig. 4).

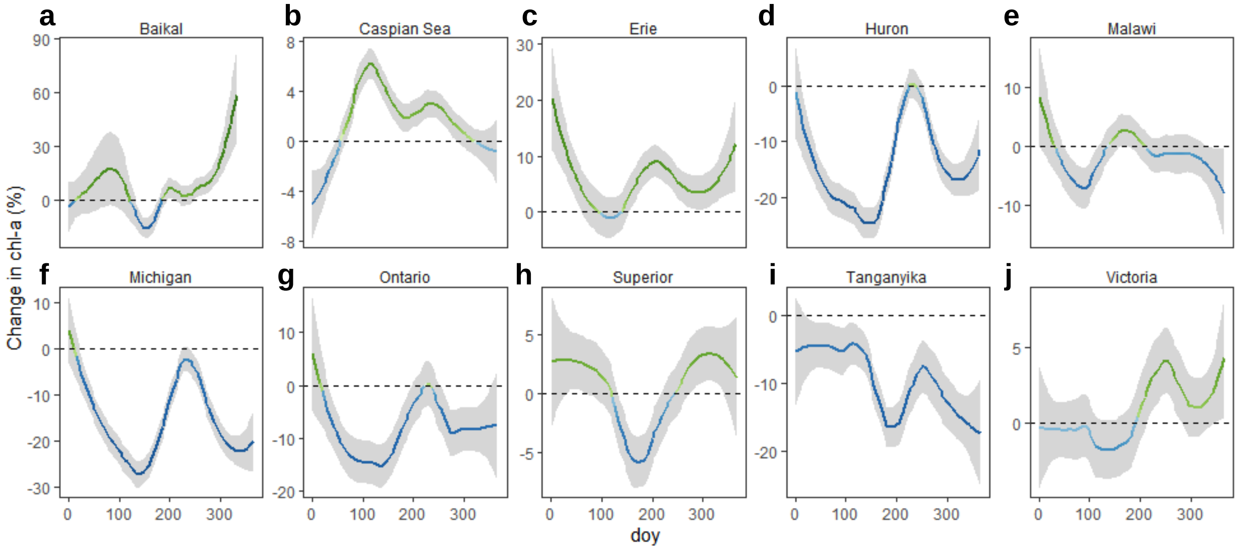

Fig. 4 | Seasonal variation in lake chl-a trends (1997-2020). Panels (**a:j**) show seasonal trends in chl-a for the 10 largest lakes with broad seasonal data coverage. Lines represent the LOESS-smoothed daily trend in chl-a weighted by the number of observations included in the chl-a trend calculation for each day of the year. The blue to green color reinforces values on the y-axes and is consistent across panels. The shaded area represents the 95% confidence interval for the smoothed line.

Overall, we provide a global view of trends in near surface chl-a over the past 23 years for large lakes. Our analysis of chl-a in lakes demonstrates the promise of spatially-explicit long-term satellite observations for tracking chl-a conditions and disentangling the multiple overlapping drivers of change. The approach used here augments the geographically and temporally limited *in situ* chl-a monitoring efforts where data is often not shared readily nor in near real time. This analysis applies a novel statistical approach to merge chl-a data from multiple sensors to produce a validated data set that documents global surface lake chl-a dynamics with new levels of spatial detail and accuracy. Global datasets documenting the aquatic concentration of chlorophyll-a (chl-a) with remote sensing can serve as a key indicator of lake responses to human activity but so far have been underused. The accuracy of remote sensing based chl-a estimates has been questioned at the local scale due to the presence of surface algae scums, submerged vegetation, sediment, and high concentrations of organic matter [44–46]. However, the cross validation and the performance of the lake-specific chl-a algorithm developed here (Supplemental Fig. S5) suggests that our main conclusions are robust to such effects. Nonetheless, we caution against the overinterpretation of specific trend estimates reported here and suggest corroborating observed trends in chl-a with *in situ* measurements wherever possible. In the frequent absence of such *in situ* measurements, remote sensing data of this type may provide the best approximation of global scale trends yet available.

Our primary result that chl-a concentrations decreased for 56% of lake area challenges the putative widespread increase in chl-a intensity that is expected due to human activity. Furthermore, we highlight that lake chl-a trends vary substantially across the surface of lakes, and across seasons making lake-wide average trends or patterns extrapolated from small central extraction points potentially misleading. The findings reported here reinforce the need for water-resource management strategies that integrate the potential for both increases and decreases in chl-a due to global change. Spatially-explicit water quality monitoring is essential for evaluating the success of investments in water management and for detecting new management challenges. Management approaches that currently treat lake-wide surface chl-a trends in a simplistic fashion should immediately benefit from the detailed maps of chl-a trends provided here. Resolving key challenges in water management requires spatially- and temporally-explicit approaches that engage policymakers and water managers at scales relevant to their decisions, including subnational administrative units, bays, and delimited stretches of lake shoreline. The data used herein hold promise for identifying the timing and magnitude of lake phytoplankton variations at daily scales allowing lake scientists and managers to concurrently capture human influences on surface water quality in near real time. The need to mobilize financial resources to support integrated approaches using these data is imperative, before additional drift from past ecological conditions becomes the new accepted norm for lakes.

Methods:

Overview

We calculated long-term (1997-2020) chl-a trends using 23 years of remote sensing data for 345 lakes (listed in Table S1). Trends were calculated from chl-a anomalies where the effects of the day of the year, latitude, longitude, and remote sensing platform as well as the interactions between these variables had been accounted for and removed from the data. We calculated a single lake-wide trend where chl-a anomalies were pooled across pixels and seasons for each lake. We also calculated separate trends for each pixel (where chl-a anomalies were pooled across all days of the year) and for each day of the year (where chl-a anomalies were pooled across pixels). The size of the pixels was 1-km for lakes in Europe and 4-km for the rest of the globe based on the limitation of the data source used here [47].

Remote sensing chl-a data

We used 742 million chl-a observations merged across 6 sensors (SeaWiFS, MODIS AQUA, MERIS, OLCI-B, VIIRS NPP, and VIIRS JPSS-1) to assess long-term trends in 345 lakes under ice-free and cloud-free conditions from year 1997 to 2020. Chl-a data were retrieved from the "CHL-OC5" product produced by GlobColour [47] and made available via the Copernicus Marine Environmental Monitoring Service (CMEMS) website: http://marine.copernicus. eu/services-portfolio/access-to-products/. The algorithm used in the CHL-OC5 data product is a five-channel chlorophyll concentration algorithm which was developed for optically complex "case II waters"[24] and has been partially validated using global *in situ* data from marine and inland waters [48–50]. We build on this validation by expanding it to in situ data from 53 lakes as described below. The daily chl-a data reflect lake environments in the near surface layer during ice-free and cloud-free conditions. Thus, the seasonal extent and the number of chl-a observations varied across lakes ranging from 2601 observations for Lake Mogotoyeyo to 365 million observations for Lake Ladoga. We downloaded and processed the chl-a values in the R environment for statistical computing[51] using the "data.table"[52], "dismo"[53], "sf"[54], "gbm"[55], "zyp"[56] and "lubridate"[57] packages. Data visualizations were made using "ggplot2"[58].

Chl-a algorithm cross validation and adaptation for inland waters

We adapted remotely sensed chl-a values specifically for lakes based on a comparison of 20,165 *in situ* chl-a measurements (filtered water samples) from 56 lakes matched to interpolated remote sensing data. To interpolate the remote sensing chl-a values, we used fully deterministic BRTs (bag fraction = 1) which modelled remotely sensed chl-a as a function of the decimal date, day of the year, sensor, latitude, and longitude separately for each lake. We used the resulting boosted regression trees (BRTs) to estimate remotely-sensed chl-a concentrations for all 6 sensors at the time and location of each *in situ* measurement. These modeled values served as the remotely-sensed matchup value for each *in situ* measurement. *In situ* data used for this purpose were downloaded, digitized, and compiled from published sources (Table S2).

We modelled the difference between *in situ* values and their remotely sensed matchup values as a function of the raw remotely sensed chl-a value, the *in situ* data source, and 3 lake characteristics (mean lake depth, surface area, and shoreline development index (a metric of shoreline complexity; the ratio of a lake's shoreline length to the circumference of a circle with the equivalent lake area)) also using a BRT. These three lake characteristic variables were used because they are associated with lake optical characteristics[59] and are freely available from the HydroLAKES database[60]. Thus, the BRT allowed the difference between *in situ* and remotely sensed chl-a values to vary from lake to lake. We then used the resulting model to estimate the difference between *in situ* and remotely sensed values for all 742 million chl-a observations used here. We translated the remotely sensed chl-a values into an "*in situ* analogue" chl-a value by subtracting the modelled differences from the raw remotely sensed values. The resulting *in situ* analogue chl-a values were used for all subsequent analyses.

Chl-a anomaly calculations

To estimate lake surface chl-a anomalies, we accounted for and removed variation in each lake's *in situ* analogue chl-a data which could be attributed to the day of the year, latitude, longitude, and sensor. This allowed us to calculate trends over time in chl-a anomalies which were not influenced by these variables or the interactions among them. We used a tree complexity of 5 to allow for high levels of interactions among variables (e.g. sensor type could have different effects on *in situ* analog chl-a at specific grid cells within lakes and at specific times of the year). To prevent model overfitting, the BRTs were fit separately for each lake 10 times using a randomly selected 50% of the data. Predicted values were generated from each of the 10 models for all observations and averaged to generate more robust estimates. The difference between the *in situ* analog chl-a values and the average of the 10 model predictions were termed, "chl-a anomalies." We confirmed that this process successfully removed the variation attributable to the day of the year, latitude, longitude, and sensor using visual diagnostic plotting for all lakes (see example for Lake Erie in Supplemental Fig. S6).

BRTs include a variety of tuning parameters which influence the model performance in cross validation. We selected a combination of tuning parameters (bag fraction = 0.62, tree complexity = 5) which reliably gave good performance in 10-fold cross validation across all lakes (median predicted residual error sum of squares = 0.35 μg L^{-1}, and median correlation between predicted and observed values = 0.85). We optimized the learning rate separately for each of the 10 BRTs for each lake by iteratively running the model with smaller and smaller learning rates (from 0.8, 0.4, 0.2, 0.1, 0.05, to 0.025) until the number of trees in the BRT which minimized the predicted deviance was greater than 1000 as suggested in previous literature [61].

Chl-a trends

We used a bootstrapped error propagation technique to estimate chl-a trends and the uncertainty in each trend. The residual errors from the BRT used for adapting remotely sensed chl-a into *in situ* analogue values were propagated into the estimate of chl-a trend uncertainty. We propagated the errors by adding a residual error (the product of a randomly selected % error residual from the BRT's error distribution and the original *in situ* analogue chl-a value) to each chl-a anomaly. Distinct residual errors were iteratively added to each chl-a anomaly value with 100 repetitions. For each repetition, Theil-Sen slopes and intercepts were calculated based on mean annual chl-a anomalies. The statistical significance of each trend was calculated as the p-value of a Spearman rank correlation test relating mean chl-a anomalies to year. The trends and their associated p-values were calculated as the average across all 100 repetitions of the Theil-Sen slope and Spearman correlation calculations.

We calculated a single lake-wide trend where chl-a anomalies were pooled across pixels and seasons for each lake. We also calculated separate trends for each pixel (where chl-a anomalies were pooled across all days of the year) and for each day of the year (where chl-a anomalies were pooled across pixels). Chl-a percent change was calculated from Theil-Sen nonparametric regression in chl-a anomalies after the effects of the day of the year, latitude, longitude, and sensor as well as the interactions between these variables had been accounted for and removed from the data. Theil-Sen nonparametric regression results were translated into a proportion change by taking the difference between the Theil-Sen modelled chl-a anomalies in 2020 and 1997 as a proportion of the lake's median chl-a *in situ* analog value. This proportion was translated into a percentage by multiplying by 100.

Acknowledgements: BMK, KK, and RA acknowledge the 2017-2018 Belmont Forum and BiodivERsA joint call for research proposals under the BiodivScen ERA-Net COFUND programme and with funding from the German Science Foundation (AD 91/22-1). MWT and RA acknowledge the funding received from Marie Sklodowska-Curie Actions (Marie Skłodowska-Curie grant agreement no. 722518) and EU-ITN MANTEL project. CM acknowledges support from the German Science Foundation (DFG) Research Training Group ConFoBi (GRK 2123/1 TPX).

Author Contributions: BMK conceived of the work, led the study, completed the analysis, and wrote the manuscript with input from all co-authors. BMK, KK, MWT, CM, and RA edited and revised the manuscript.

Competing Interest Statement: The authors declare that they have no known competing financial interests or personal relationships that could have appeared to influence the work reported in this paper.

Data Availability Statement: GlobColour data (http://globcolour.info) used in this study has been developed, validated, and distributed by ACRI-ST, France. Geospatial and morphometric data for each lake is available from the previously published HydroLAKES database under the identifier doi: 10.1038/ncomms13603 and can be found at http://www.hydrosheds.org.

Code Availability Statement: All code used here are available under the identifier, DOI: 10.5281/zenodo.5026693

References:

1. Oliver, S. K. *et al.* Unexpected stasis in a changing world: Lake nutrient and chlorophyll trends since 1990. *Glob. Change Biol.* **23**, (2017).
2. Ho, J. C., Michalak, A. M. & Pahlevan, N. Widespread global increase in intense lake phytoplankton blooms since the 1980s. *Nature* **574**, 667–670 (2019).
3. Yvon-Durocher, G. *et al.* Five Years of Experimental Warming Increases the Biodiversity and Productivity of Phytoplankton. *PLoS Biol.* **13**, (2015).
4. Woolway, R. I. & Merchant, C. J. Worldwide alteration of lake mixing regimes in response to climate change. *Nat. Geosci.* **12**, 271–276 (2019).
5. Kosten, S. *et al.* Warmer climates boost cyanobacterial dominance in shallow lakes. *Glob. Change Biol.* **18**, 118–126 (2012).
6. Wagner, C. & Adrian, R. Cyanobacteria dominance: Quantifying the effects of climate change. *Limnol. Oceanogr.* **54**, 2460–2468 (2009).
7. Paerl, H. W. & Paul, V. J. Climate change: links to global expansion of harmful cyanobacteria. *Water Res.* **46**, 1349–63 (2012).

8. Rigosi, A., Carey, C. & Ibelings, B. The interaction between climate warming and eutrophication to promote cyanobacteria is dependent on trophic state and varies among taxa. *Limnol. Oceanogr.* **59**, 99–114 (2014).
9. Dodds, W. K. *et al.* Eutrophication of U.S. Freshwaters: Analysis of Potential Economic Damages. *Environ. Sci. Technol.* **43**, 12–19 (2009).
10. O'Reilly, C. M., Alin, S. R., Plisnier, P.-D., Cohen, A. S. & McKee, B. A. Climate change decreases aquatic ecosystem productivity of Lake Tanganyika, Africa. *Nature* **424**, 766–8 (2003).
11. Tierney, J. E. *et al.* Late-twentieth-century warming in Lake Tanganyika unprecedented since AD 500. *Nat. Geosci.* **3**, 422–425 (2010).
12. Behrenfeld, M. J. *et al.* Climate-driven trends in contemporary ocean productivity. *Nature* **444**, 752–755 (2006).
13. Michelutti, N. *et al.* Climate change forces new ecological states in tropical Andean lakes. *PLoS ONE* **10**, e0115338 (2015).
14. Kraemer, B. M., Mehner, T. & Adrian, R. Reconciling the opposing effects of warming on phytoplankton biomass in 188 large lakes. *Sci. Rep.* **7**, (2017).
15. Yvon-Durocher, G., Montoya, J. M., Trimmer, M. & Woodward, G. Warming alters the size spectrum and shifts the distribution of biomass in freshwater ecosystems. *Glob. Change Biol.* **17**, 1681–1694 (2011).
16. Kraemer, B. M. *et al.* Global patterns in lake ecosystem responses to warming based on the temperature dependence of metabolism. *Glob. Change Biol.* **23**, 1881–1890 (2017).
17. Vanderploeg, H. A. *et al. Dispersal and emerging ecological impacts of Ponto-Caspian species in the Laurentian Great Lakes*. *Canadian Journal of Fisheries and Aquatic Sciences* vol. 59 (2002).

18. Warner, D. M. & Lesht, B. M. Relative importance of phosphorus, invasive mussels and climate for patterns in chlorophyll a and primary production in Lakes Michigan and Huron. *Freshw. Biol.* **60**, 1029–1043 (2015).

19. Jeppesen, E. *et al.* Lake responses to reduced nutrient loading - An analysis of contemporary long-term data from 35 case studies. *Freshw. Biol.* **50**, 1747–1771 (2005).

20. Evans, M. A., Fahnenstiel, G. & Scavia, D. Incidental oligotrophication of North American Great Lakes. *Environ. Sci. Technol.* **45**, 3297–3303 (2011).

21. Anderson, N. J., Jeppesen, E. & Søndergaard, M. Ecological effects of reduced nutrient loading (oligotrophication). An introduction. *Freshwat Biol* **50**, 1589–1593 (2005).

22. Vörösmarty, C. J. *et al.* Global threats to human water security and river biodiversity. *Nature* **467**, 555–561 (2010).

23. Kraemer, B. M. Rethinking discretization to advance limnology amid the ongoing information explosion. *Water Res.* **178**, 115801 (2020).

24. Gohin, F., Druon, J. N. & Lampert, L. A five channel chlorophyll concentration algorithm applied to Sea WiFS data processed by SeaDAS in coastal waters. *Int. J. Remote Sens.* **23**, 1639–1661 (2002).

25. Blukacz, E. A., Sprules, W. G. & Brunner, J. Use of the bootstrap for error propagation in estimating zooplankton production. *Ecology* **86**, 2223–2231 (2005).

26. Vammen, K., Pitty, J. & Montenegro Guillén, S. Evaluación del proceso de eutroficación del lago Cocibolca, Nicaragua y sus causas en la cuenca. *En Eutrofización En América Sur Consecuencias Tecnol. Gerenc. Control Inst. Int. Ecol. Interacademic Panel Int. Issues* 35–58 (2006).

27. Cohen, A. S. *et al.* Climate warming reduces fish production and benthic habitat in Lake Tanganyika, one of the most biodiverse freshwater ecosystems. *Proc. Natl. Acad. Sci.* **113**, 9563–9568 (2016).

28. Rugema, E. *et al.* Long-term change of phytoplankton in Lake Kivu: The rise of the greens. *Freshw. Biol.* **64**, 1940–1955 (2019).

29. Michalak, A. M. *et al.* Record-setting algal bloom in Lake Erie caused by agricultural and meteorological trends consistent with expected future conditions. *Proc. Natl. Acad. Sci.* **110**, 6448–6452 (2013).

30. Rukhovets, L. A. *et al.* Studying the response of Lake Ladoga ecosystem to a decrease in phosphorus load. *Water Resour.* **38**, 806–817 (2011).

31. Kuhn, C. & Butman, D. Declining greenness in Arctic-boreal lakes. *Proc. Natl. Acad. Sci.* **118**, e2021219118 (2021).

32. Sommer, U. & Lewandowska, A. Climate change and the phytoplankton spring bloom: warming and overwintering zooplankton have similar effects on phytoplankton. *Glob. Change Biol.* **17**, 154–162 (2011).

33. O'Connor, M. I. M., Piehler, M. F. M., Leech, D. M. D., Anton, A. & Bruno, J. F. Warming and resource availability shift food web structure and metabolism. *PLoS Biol.* **7**, e1000178 (2009).

34. Kraemer, B. M. *et al.* Morphometry and average temperature affect lake stratification responses to climate change. *Geophys. Res. Lett.* **42**, 4981–4988 (2015).

35. Richardson, D. C. *et al.* Transparency, geomorphology and mixing regime explain variability in trends in lake temperature and stratification across Northeastern North America (1975-2014). *Water Switz.* **9**, (2017).

36. Winder, M. & Sommer, U. Phytoplankton response to a changing climate. *Hydrobiologia* **698**, 5–16 (2012).

37. Multi-decadal improvement in US Lake water clarity - IOPscience. https://iopscience.iop.org/article/10.1088/1748-9326/abf002/meta.

38. Wilkinson, G., Walter, J. A., Buelo, C. & Pace, M. No evidence of widespread algal bloom intensification in hundreds of lakes. in (AGU, 2020).

39. Modabberi, A. *et al.* Caspian Sea is eutrophying: the alarming message of satellite data. *Environ. Res. Lett.* **15**, 124047 (2020).

40. Stow, C. A. *et al.* Phosphorus targets and eutrophication objectives in Saginaw Bay: A 35year assessment. *J. Gt. Lakes Res.* **40**, 4–10 (2014).

41. Archundia, D. *et al.* How uncontrolled urban expansion increases the contamination of the titicaca lake basin (El Alto, La Paz, Bolivia). *Water. Air. Soil Pollut.* **228**, 44 (2017).

42. Ignatieva, N. V. Distribution and release of sedimentary phosphorus in Lake Ladoga. *Hydrobiologia* **322**, 129–136 (1996).

43. Woolway, R. I. *et al.* Phenological shifts in lake stratification under climate change. *Nat. Commun.* **12**, 2318 (2021).

44. Feng, L. *et al.* Concerns about phytoplankton bloom trends in global lakes. *Nature* **590**, E35–E47 (2021).

45. Palmer, S. C. J., Kutser, T. & Hunter, P. D. Remote sensing of inland waters: Challenges, progress and future directions. *Remote Sens. Environ.* **157**, 1–8 (2015).

46. Matthews, M. W. A current review of empirical procedures of remote sensing in inland and near-coastal transitional waters. *Int. J. Remote Sens.* **32**, 6855–6899 (2011).

47. Maritorena, S., d'Andon, O. H. F., Mangin, A. & Siegel, D. A. Merged satellite ocean color data products using a bio-optical model: Characteristics, benefits and issues. *Remote Sens. Environ.* **114**, 1791–1804 (2010).

48. Gbagir, A.-M. G. & Colpaert, A. Assessing the Trend of the Trophic State of Lake Ladoga Based on Multi-Year (1997–2019) CMEMS GlobColour-Merged CHL-OC5 Satellite Observations. *Sensors* **20**, 6881 (2020).

49. Pitarch, J., Volpe, G., Colella, S., Krasemann, H. & Santoleri, R. Remote sensing of chlorophyll in the Baltic Sea at basin scale from 1997 to 2012 using merged multi-sensor data. *Ocean Sci.* **12**, 379–389 (2016).
50. Lavigne, H. *et al.* Quality-control tests for OC4, OC5 and NIR-red satellite chlorophyll-a algorithms applied to coastal waters. *Remote Sens. Environ.* **255**, 112237 (2021).
51. R Core Team. *R: A Language and Environment for Statistical Computing*. *R Foundation for Statistical Computing* (R Foundation for Statistical Computing, 2020).
52. Dowle, M. *et al.* Package 'data. table'. *Ext. 'data Frame* (2019).
53. Hijmans, R. J., Phillips, S., Leathwick, J., Elith, J. & Hijmans, M. R. J. Package 'dismo'. *Circles* **9**, 1–68 (2017).
54. Pebesma, E. J. Simple features for R: Standardized support for spatial vector data. *R J* **10**, 439 (2018).
55. Ridgeway, G. & Ridgeway, M. G. The gbm package. *R Found. Stat. Comput. Vienna Austria* **5**, (2004).
56. Bronaugh, D., Werner, A. & Bronaugh, M. D. Package 'zyp'. *CRAN Repos.* (2009).
57. Grolemund, G. & Wickham, H. Dates and times made easy with lubridate. *J. Stat. Softw.* **40**, 1–25 (2011).
58. Wickham, H. *ggplot2: Elegant Graphics for Data Analysis*. (Springer-Verlag New York, 2009).
59. Eleveld, M. A. *et al.* An optical classification tool for global lake waters. *Remote Sens.* **9**, (2017).
60. Messager, M. L., Lehner, B., Grill, G., Nedeva, I. & Schmitt, O. Estimating the volume and age of water stored in global lakes using a geo-statistical approach. *Nat. Commun.* **7**, (2016).
61. Elith, J., Leathwick, J. & Hastie, T. A working guide to boosted regression trees. *J. Anim. Ecol.* **77**, 802–813 (2008).

Supplemental Figures:

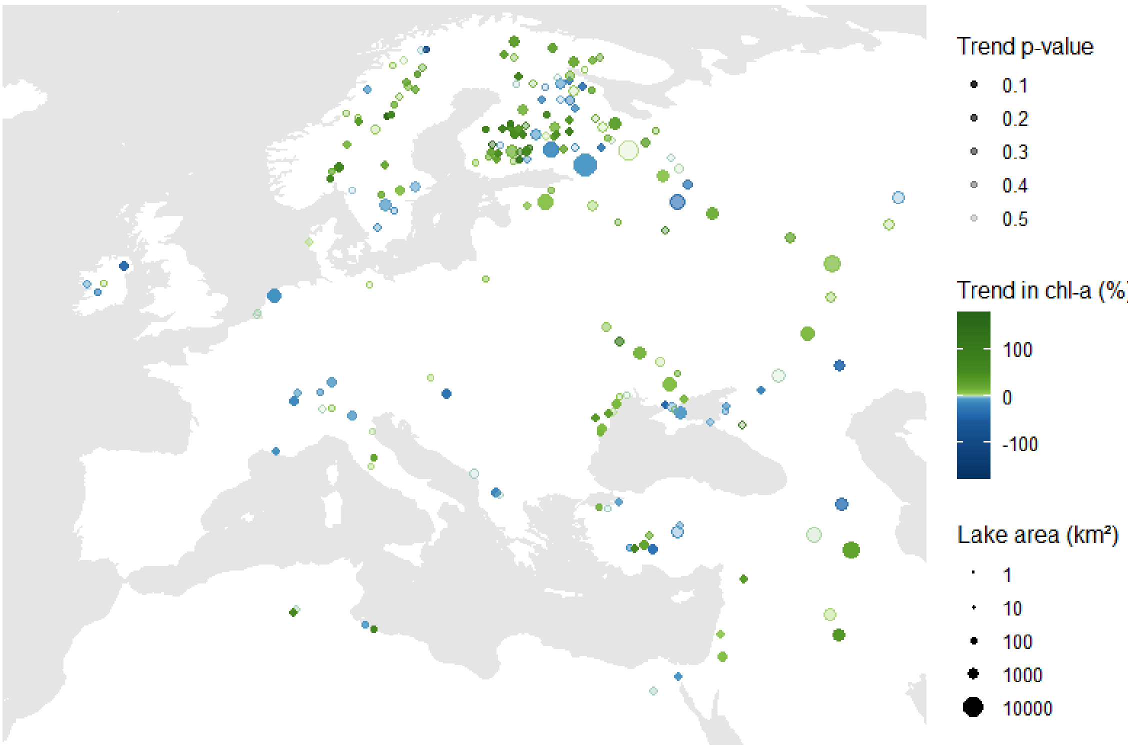

Supplemental Fig. S1 | Chl-a percent change (1997-2020) based on lake-wide averages for European lakes with data at higher spatial resolution (1 km x 1 km). The color of the dot indicates the trend with green values corresponding to increases in chl-a and blue values corresponding to decreases in chl-a. The opacity of the trend is proportional to its significance with more opaque circles indicating more statistically significant trends. The size of the dot is proportional to the area of each lake.

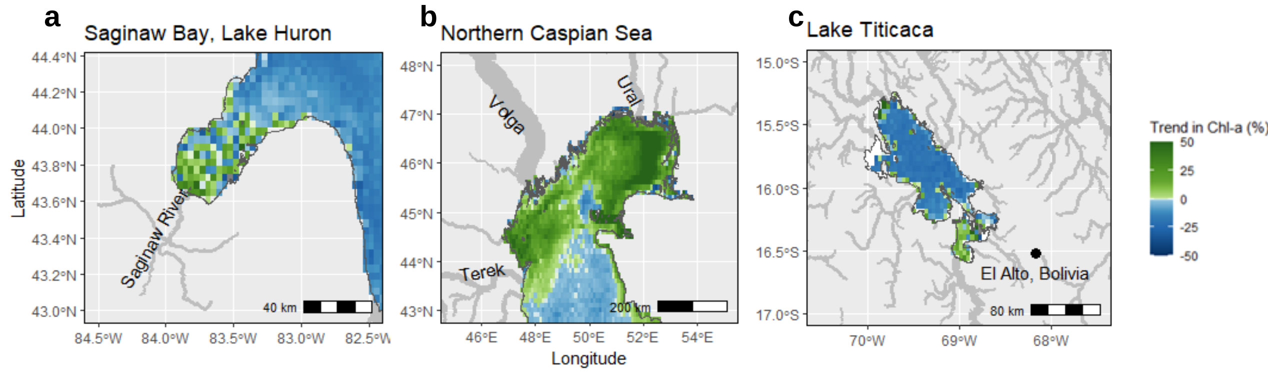

Supplemental Fig. S2 | Greening near the mouths of major inflowing rivers. Maps shown for Saginaw Bay, Lake Huron (**a**), the Northern Caspian Sea (**b**), and Lake Titicaca (**c**).

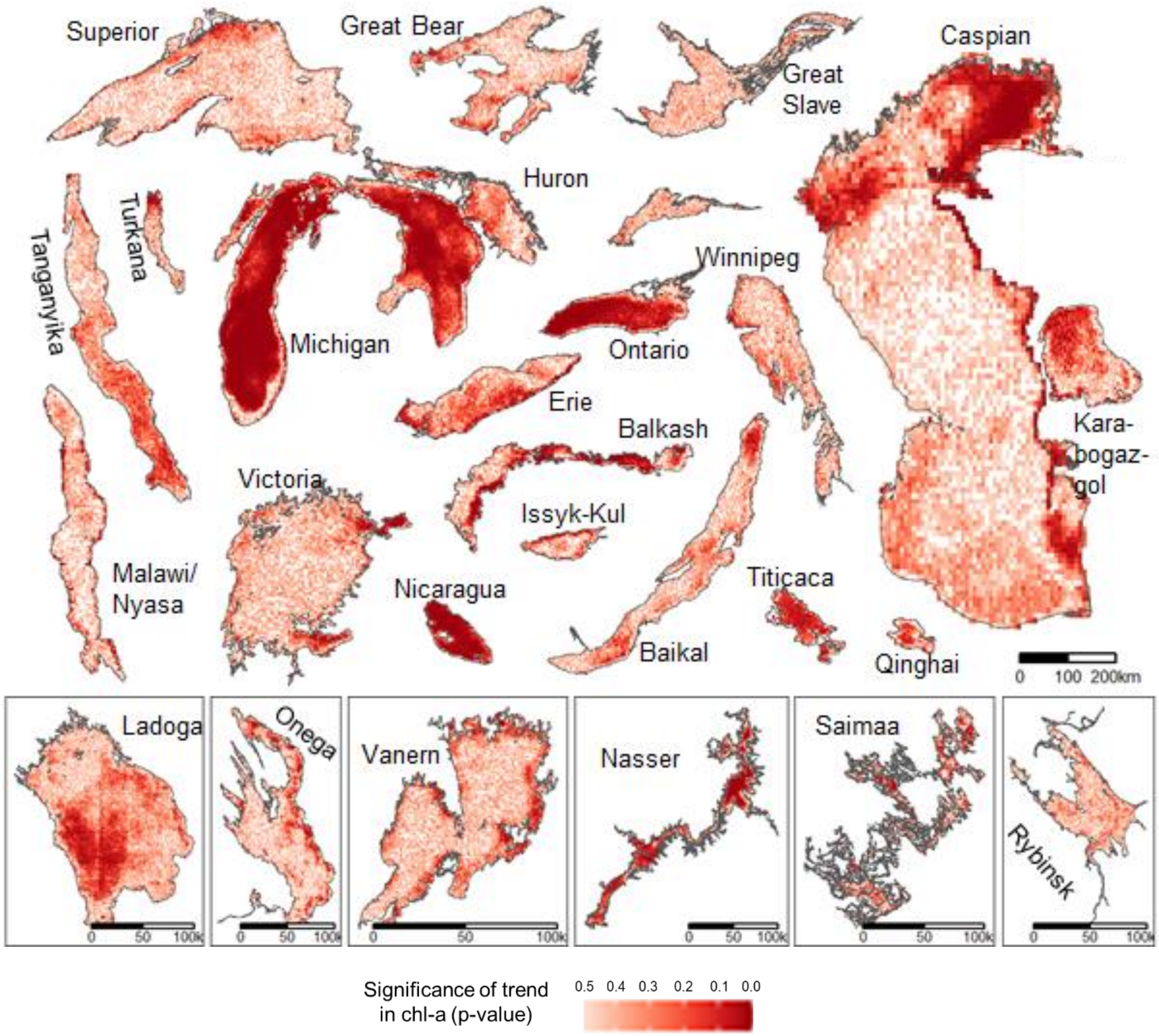

Supplemental Fig. S3 | Statistical significance of trends across space within lakes. Lakes shown are the same as those in Fig 3. Darker reds indicate relatively higher statistical significance. P-values less than 0.5 appear white.

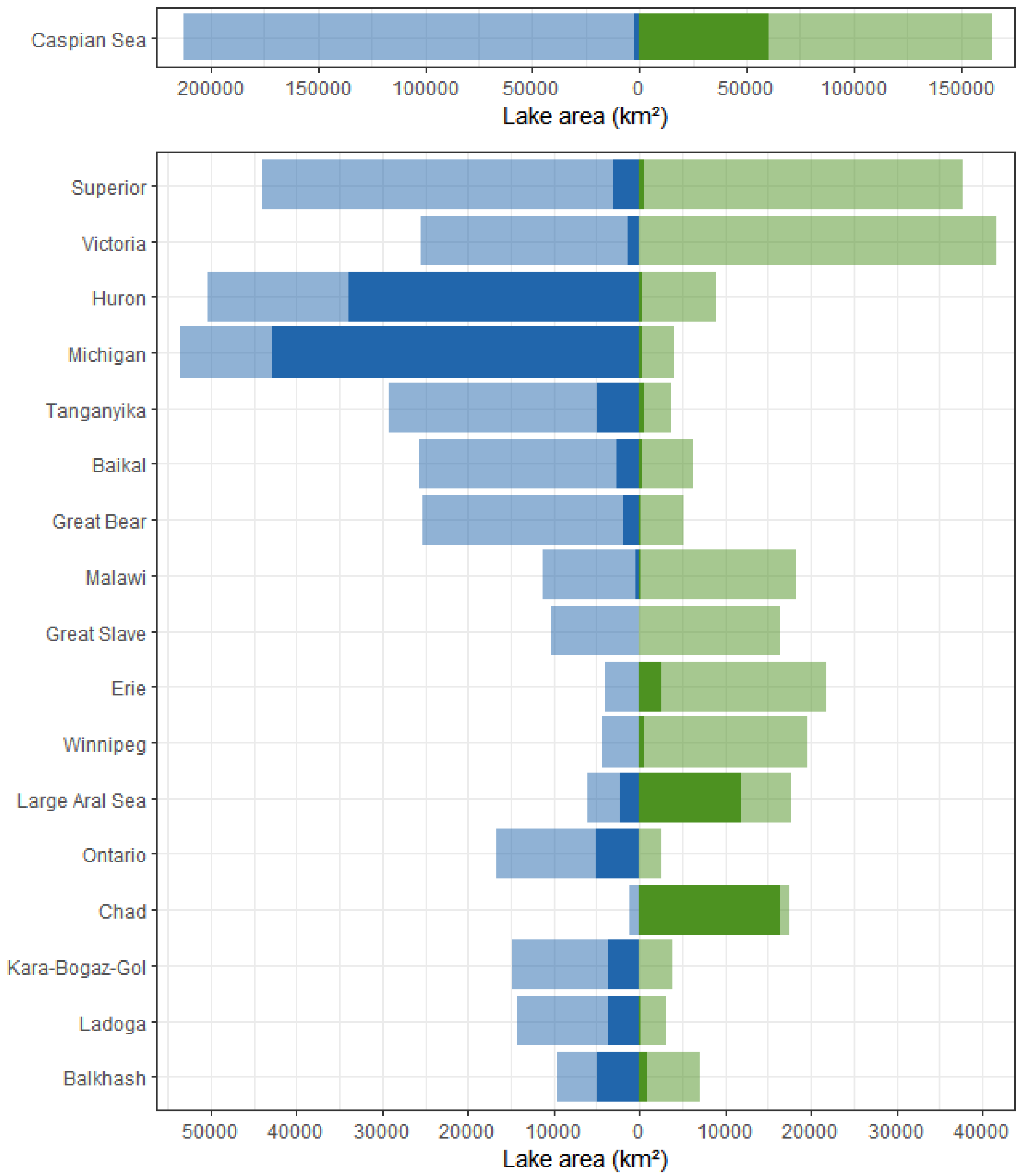

Supplemental Fig. S4 | The proportion of lake area which exhibited decreases (blue bars) versus increases (green bars) in chl-a for the largest 18 lakes in the world. The darker portion of each bar represents the proportion of lake area which had significant trends at the α = 0.1 level. The Caspian Sea is plotted separately to facilitate visualization of the smaller lakes which are plotted on a separate x-axis scale.

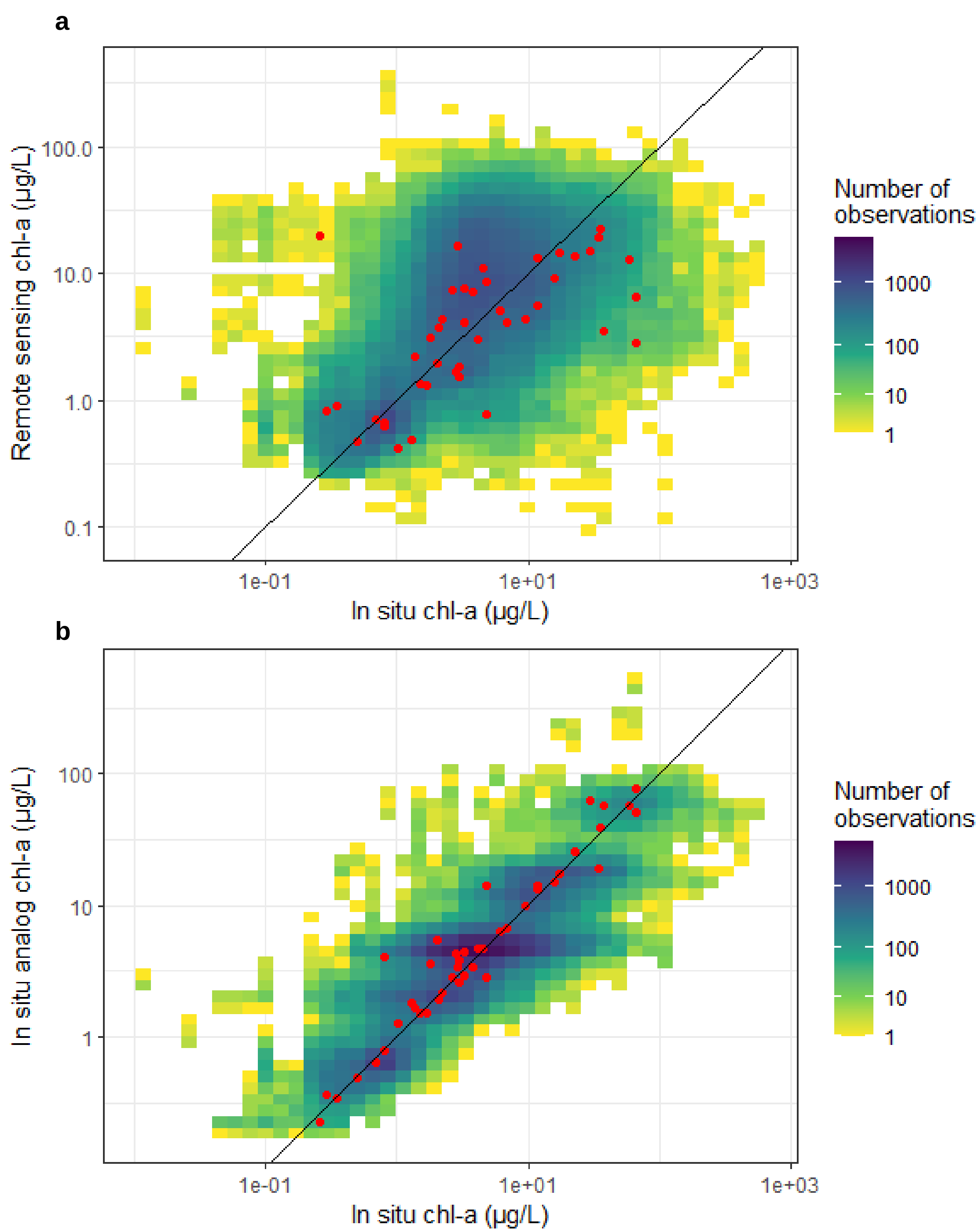

Supplemental Fig. S5 | Cross validation of remotely sensed chl-a. Relationship between *in situ* chl-a and the nearest raw remote sensing chl-a value (**a**). Relationship between *in situ* chl-a and the *in situ* analogue chl-a values after adapting the chl-a algorithm for specific lakes according to their characteristics (**b**). The shaded area reflects the density of the chl-a observations at each gridcell. The red dots are the lake-wide averages for each of the 56 lakes where *in situ* chl-a data were available.

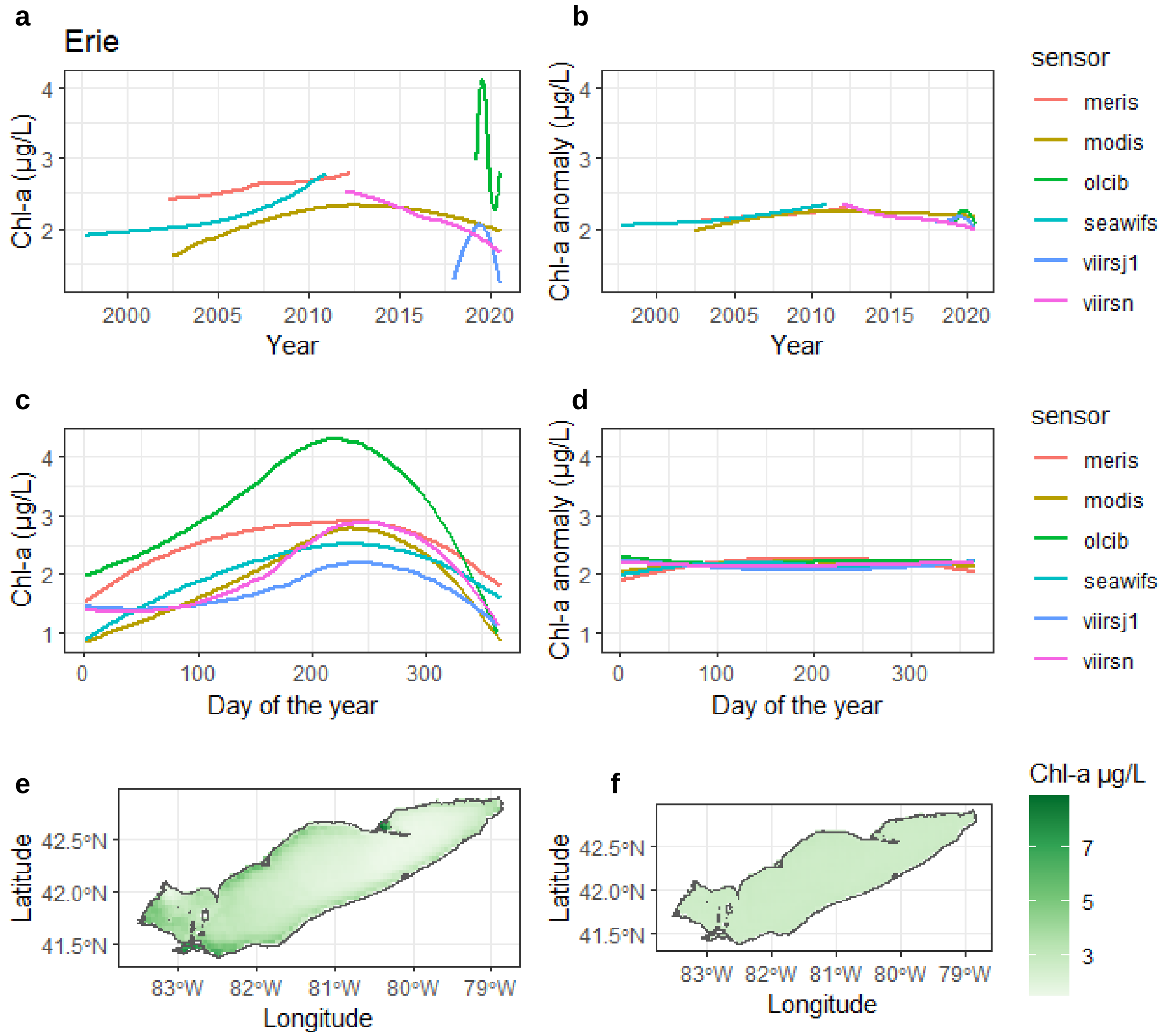

Supplemental Fig. S6 | Calculation of chl-a anomalies from *in situ* analog chl-a values. We used boosted regression trees to remove the variation in chl-a (*in situ* analog values) attributable to the sensor (**a**, **b**), the day of the year (**c**, **d**), and the location (latitude and longitude) (**e**, **f**). Locally weighted scatterplot smoothing (LOWESS) lines are shown for raw chl-a values (**a, c, e**) and chl-a anomaly values (**b, d, f**) demonstrating that the variation attributable to three variables (sensor, day of the year, and location) and their interactions was successfully removed by this method.

Supplemental Table S1 | List of all large lakes included in the analysis including their characteristics.

Supplemental Table S2 | *In situ* chl-a data used for chl-a algorithm tuning.